Stem Cell Reports
Article

ISSCR

OPEN ACCESS

Endogenous DNA Damage Leads to p53-Independent Deficits in Replicative Fitness in Fetal Murine *Fancd2*$^{-/-}$ Hematopoietic Stem and Progenitor Cells

Young me Yoon,[1,2,3] Kelsie J. Storm,[1,2,3,5] Ashley N. Kamimae-Lanning,[1,2,3,6] Natalya A. Goloviznina,[1,2,3,7] and Peter Kurre[1,2,3,4,*]

[1]Department of Pediatrics
[2]Papé Family Pediatric Research Institute
[3]Pediatric Cancer Biology Program
Oregon Health & Science University, Portland, OR 97239, USA
[4]OHSU Knight Cancer Institute, Oregon Health & Science University, 3181 Southwest Sam Jackson Park Road, Portland, OR 97239, USA
[5]Present address: Randall Children's Hospital, Portland, OR 97227, USA
[6]Present address: MRC Laboratory of Molecular Biology, Protein & Nucleic Acids Division, Cambridge CB2 0QH, UK
[7]Present address: Molecular, Cellular, and Structural Biology, University of Minnesota, Minneapolis, MN 55455, USA
*Correspondence: kurrepe@ohsu.edu
http://dx.doi.org/10.1016/j.stemcr.2016.09.005

SUMMARY

Our mechanistic understanding of Fanconi anemia (FA) pathway function in hematopoietic stem and progenitor cells (HSPCs) owes much to their role in experimentally induced DNA crosslink lesion repair. In bone marrow HSPCs, unresolved stress confers p53-dependent apoptosis and progressive cell attrition. The role of FA proteins during hematopoietic development, in the face of physiological replicative demand, remains elusive. Here, we reveal a fetal HSPC pool in *Fancd2*$^{-/-}$ mice with compromised clonogenicity and repopulation. Without experimental manipulation, fetal *Fancd2*$^{-/-}$ HSPCs spontaneously accumulate DNA strand breaks and RAD51 foci, associated with a broad transcriptional DNA-damage response, and constitutive activation of ATM as well as p38 stress kinase. Remarkably, the unresolved stress during rapid HSPC pool expansion does not trigger p53 activation and apoptosis; rather, it constrains proliferation. Collectively our studies point to a role for the FA pathway during hematopoietic development and provide a new model for studying the physiological function of FA proteins.

INTRODUCTION

Fanconi anemia (FA) is a recessively inherited, multisystem disorder characterized by congenital anomalies, hematopoietic failure, and cancer predisposition (Kutler et al., 2003). Biallelic mutations in one of at least 22 identified FA genes (with the exception of X-linked *FANCB*) result in progressive stem cell attrition in 90% of affected patients (Kee and D'Andrea, 2012). Human and murine FA hematopoietic stem and progenitor cells (HSPCs) exhibit characteristic susceptibility to DNA-crosslinking agents (Knipscheer et al., 2009) and chronic inflammatory stimulation (Hu et al., 2013; Rathbun et al., 1997), as well as an exaggerated sensitivity to aldehydes when canonical elimination pathways are disabled (Garaycoechea and Patel, 2014; Pontel et al., 2015). Yet the physiological role of FA proteins in maintaining HSPC pool size remains to be clarified, owing, in part, to a lack of model systems that mimic the spontaneous and progressive hematopoietic failure seen in patients (Garaycoechea and Patel, 2014; Walter et al., 2015).

To gain insight into the role of FA proteins during development and understand the origin of HSPC deficits, we recently investigated fetal hematopoietic function in a murine model of FA, observing quantitative hematopoietic deficits at embryonic day 14.5 (E14.5) (Kamimae-Lanning et al., 2013). This is consistent with a case report of compromised cord blood clonogenicity and observations of decreased bone marrow progenitor content in young FA patients (Auerbach et al., 1990; Ceccaldi et al., 2012). Indeed, rapid proliferation during experimental transplantation of murine FA bone marrow, progenitor proliferation in rapidly dividing FANCD2- and FANCA-depleted human embryonic stem cells (Tulpule et al., 2010), or primordial germ cell turnover (Luo et al., 2014) all reveal proliferation deficits following replication stress. During development, definitive murine HSPCs experience a rapid 33-fold expansion in the fetal liver (FL) between E12.5 and E16.5 (Ema and Nakauchi, 2000; Mikkola and Orkin, 2006), after which hematopoietic function transitions to the bone marrow where HSPCs assume a more quiescent postnatal phenotype (Copley et al., 2013; Morrison and Spradling, 2008).

HSPCs have evolved complex regulatory systems to minimize DNA damage accrued in response to endogenous and exogenous compounds or associated with aging (Bakker and Passegue, 2013; Flach et al., 2014; Lindahl, 1993). The FA pathway appears to shift double-strand-break repair away from the more error-prone non-homologous end-joining (NHEJ) repair pathway (Kottemann and Smogorzewska, 2013; Zhang et al., 2016). Components of the alternative homologous combination (HR) pathway are critical to progenitor repair integrity, suggesting that the disruption of the FA pathway would leave the progenitor pool especially vulnerable to damage accrual (Mohrin et al.,

A

		Fancd2 +/+	*Fancd2* +/-	*Fancd2* -/-	Total
12.5 dpc	n	20	31	11	62
	%	32.3	50.0	17.7	100
14.5 dpc	n	75	173	57	305
	%	24.6	56.7	18.7	100

B

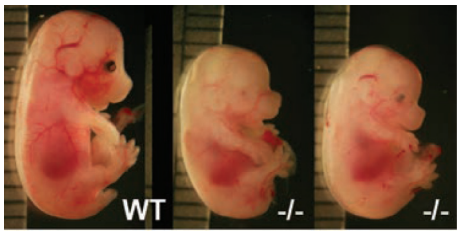

C

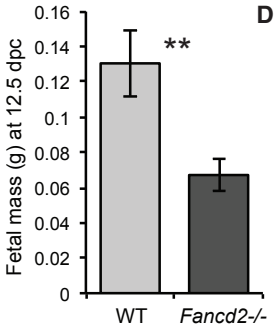

D

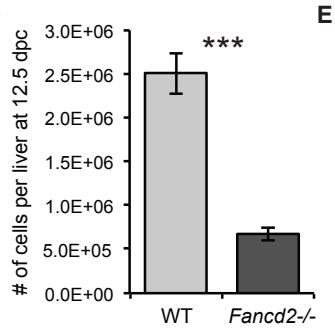

E

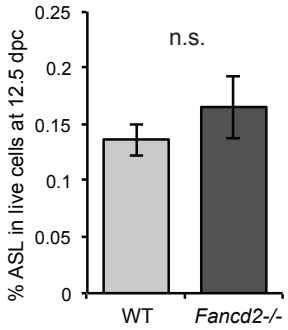

F

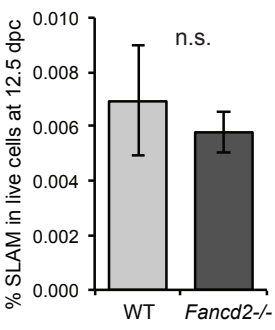

G

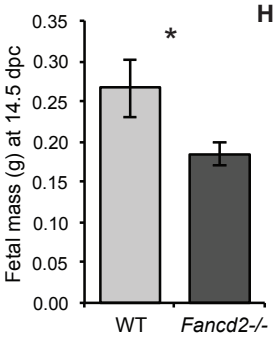

H

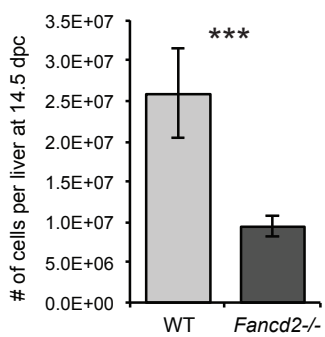

I

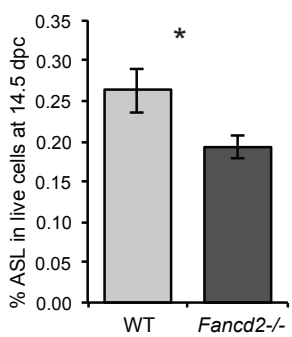

J

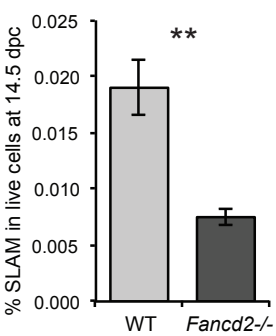

K

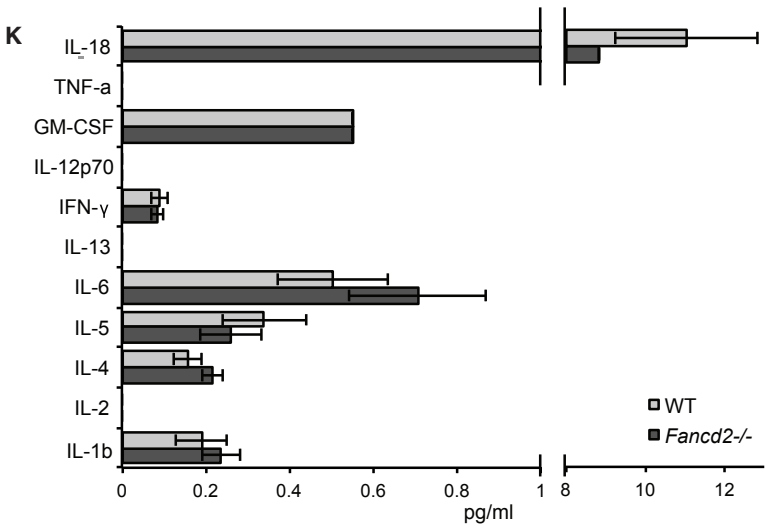

(legend on next page)

2010). Recent studies further suggest that protective mechanisms are required to balance the physiological replicative stress that coincides with rapid cell division during hematopoietic development (Alvarez et al., 2015; Copley et al., 2013; Mikkola and Orkin, 2006).

Thus, fetal hematopoiesis provides a unique opportunity to test the hypothesis that FA proteins have a physiological, alkylator-independent role in guarding against replication stress during development, preventing attrition in the rapidly cycling fetal HSPC pool (Lossaint et al., 2013; Luebben et al., 2014). Our data from *Fancd2*$^{-/-}$ FL HSPC herein reveal deficits in proliferative fitness and a broad damage response with constitutive activation of p38, but no evidence of the characteristic postnatal p53 response or apoptosis.

RESULTS

Fancd2$^{-/-}$ Fetuses Exhibit Pervasive Developmental Defects and a Deficiency of Fetal Liver HSPCs

To investigate the prenatal role of the FA pathway, we chose a model of *Fancd2* deficiency, a critical component in the coordination of downstream nuclear DNA repair events (Grompe and D'Andrea, 2001; Zhang et al., 2010). FL cells were obtained from wild-type (WT) and *Fancd2*-deficient embryos from *Fancd2*$^{+/-}$ timed breeders at 12.5 and 14.5 days post coitum (dpc). We characterized FL HSPCs at each time point by immunophenotypic analysis of ASL ($AA4.1^{+}SCA1^{+}Lin^{low/-}$) and SLAM ($CD150^{+}CD48^{-}Lin^{neg}SCA1^{+}$) cells (Kiel et al., 2005; Kim et al., 2006; Yilmaz et al., 2006). *Fancd2*$^{-/-}$ fetuses were present at a sub-Mendelian frequency at both time points, comprising 17.7%–18.7% of the total fetuses (Figure 1A) but only 9% of weanlings (Q. Zhang, personal communication), indicating an association with both early and late gestational lethality. Notably, *Fancd2*$^{-/-}$ fetuses often exhibited gross abnormalities such as microcephaly and microphthalmia (Figure 1B). At 12.5 dpc, *Fancd2*$^{-/-}$ fetuses exhibited a 51% deficit in FL mass along with a 27% decline in liver cellularity relative to WT (Figures 1C and 1D). Not surprisingly, the overall number of both ASL and SLAM HSPCs was reduced in *Fancd2*$^{-/-}$ FL even as their respective frequencies remained comparable with WT (Figures 1E and 1F). The underlying lack of FL cell expansion is readily apparent at 14.5 dpc. The *Fancd2*$^{-/-}$ fetuses were 31% smaller (Figure 1C) and their livers had 64% fewer cells than WT (Figure 1D), an even more significant proportional deficit than at the earlier time point. Strikingly, by 14.5 dpc the ASL and SLAM hematopoietic stem cell (HSC) frequencies were significantly lower in *Fancd2*$^{-/-}$ FL compared with WT, comprising 27% and 61%, respectively (Figures 1I and 1J). Whereas adult *Fancc*$^{-/-}$ HSPC show an exaggerated susceptibility to inflammation, a Luminex screening of key inflammatory cytokines showed only modest increases in interleukin-6 (IL-6) and IL-4 release from *Fancd2*$^{-/-}$ ASL FL at 14.5 dpc (Figure 1K), generally consistent with FA patient immunological profiles (Korthof et al., 2013).

Fancd2$^{-/-}$ Fetal Liver HSPCs Are Irreversibly Compromised and Exhibit Characteristic Sensitivity to DNA-Crosslinking Agents

To assess the hematopoietic progenitor cell content in *Fancd2*$^{-/-}$ FL, we conducted methylcellulose colony-formation assays from both *Fancd2*$^{-/-}$ and WT unfractionated FL, with and without the addition of a DNA interstrand crosslinker, mitomycin C (MM-C). At 12.5 dpc, WT and *Fancd2*$^{-/-}$ FLs formed 77 and 72 colonies on average with no statistical difference (Figure 2A). In the analyses with FLs at 14.5 dpc, both WT and *Fancd2*$^{-/-}$ FL formed fewer colonies compared with the FLs at 12.5 dpc. Moreover, *Fancd2*$^{-/-}$ FL formed significantly fewer colonies than WT, even in the absence of MM-C, consistent with the notion that progenitor depletion occurs in this model unprovoked by exposure to exogenous agents. These findings were exacerbated with MM-C, which reduced output from both WT and *Fancd2*$^{-/-}$ FL, but more significantly affected formation of *Fancd2*$^{-/-}$ FL colonies (Figure 2B). This phenotype persisted into adulthood (Figure 2C). We next performed serial transplantation assays, injecting unfractionated WT and *Fancd2*$^{-/-}$ CD45.2 donor FL into

Figure 1. *Fancd2*$^{-/-}$ Fetal Mice Have a Significantly Diminished Hematopoietic Compartment and Fewer HSCs

(A) Offspring yields of each genotype at 12.5 and 14.5 days post coitum (dpc) from *Fancd2*$^{+/-}$ × *Fancd2*$^{+/-}$ crosses.

(B) Common craniofacial defects seen in *Fancd2*$^{-/-}$ fetal mice.

(C–F) Characterizations of WT and *Fancd2*$^{-/-}$ fetal mice at 12.5 dpc: fetus weight ($p = 0.01$), liver cellularity ($p < 0.001$), percentage of ASL HSPCs, and percentage of SLAM HSCs in live FL cells (n = 8 WT and 7 knockout [KO] from four litters).

(G–J) Characterizations of WT and *Fancd2*$^{-/-}$ fetal mice at 14.5 dpc: fetus weight ($p = 0.04$, n = 7 WT and 8 KO from five litters), liver cellularity ($p = 0.001$, n = 7 WT and 14 KO from five litters), percentage of ASL HSPCs ($p = 0.03$, n = 10 WT and 11 KO from five litters), and percentage of SLAM HSCs in live FL cells ($p = 0.01$, n = 4 WT and 3 KO from two2 litters).

(K) Cytokine profiling of ASL-sorted WT and *Fancd2*$^{-/-}$ unfractionated FL cells (n = 3 WT and 5 KO from two litters; samples that yielded lower than the detection threshold are excluded, hence a statistical test could not be performed).

Error bars reflect SEM, and asterisks indicate *$p \leq 0.05$, **$p \leq 0.01$, and ***$p \leq 0.001$. n.s., not significant.

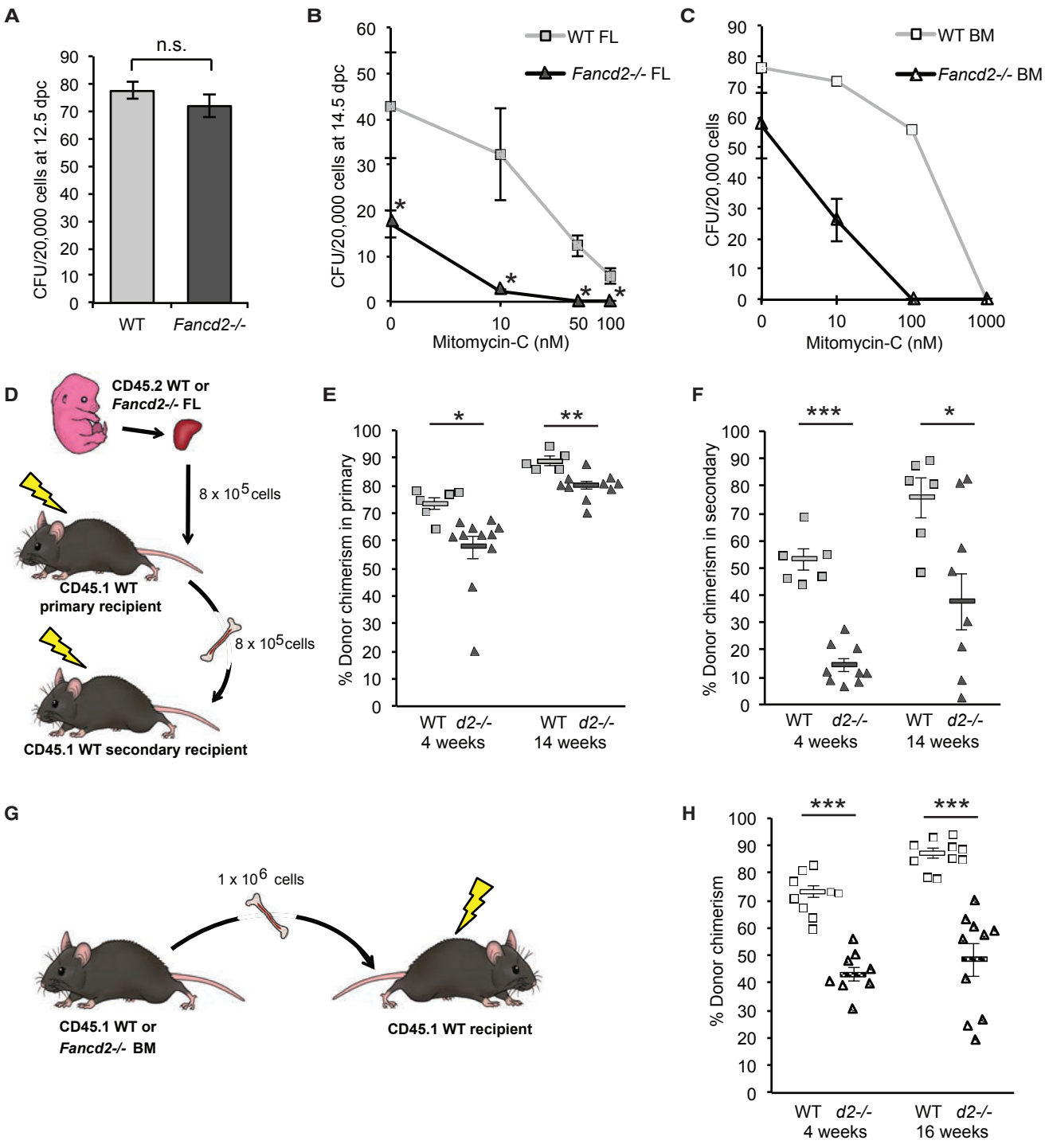

Figure 2. Defects in *Fancd2*$^{-/-}$ HSPC Frequency and Repopulating Capacity Persist from Fetal Development through Adulthood

(A) Colony-forming units per 20,000 unfractionated FL cells at 12.5 dpc (n = 5 WT and 3 KO from two litters).

(B) Colony-forming units per 20,000 unfractionated FL cells at 14.5 dpc with different doses of mitomycin C treatment ($p < 0.05$ between WT and *Fancd2*$^{-/-}$ at each concentration of MM-C, n = 5–6 WT per condition and 4–6 KO per condition from five litters).

(C) Colony-forming units per 20,000 adult whole bone marrow cells (n = 2 WT and 4 KO).

(legend continued on next page)

congenic CD45.1, sublethally irradiated recipients (Figure 2D). Primary recipients of *Fancd2*$^{-/-}$ FL cells exhibited a 22% decrease in peripheral blood donor chimerism at 4 weeks and a 10% decrease in peripheral blood donor chimerism at 14 weeks, compared with WT (Figure 2E). This proliferation deficit was further aggravated by a second round of transplantation using unfractionated bone marrow from primary transplant recipients, revealing a 73% decrease in peripheral blood donor chimerism at 4 weeks from *Fancd2*$^{-/-}$ grafts, which persisted through 14 weeks, in comparison with WT (Figure 2F). Similarly, HSPC-repopulating defects in adult bone marrow can be uncovered with the stress of transplantation, prompting a significant decrease of 42% in *Fancd2*$^{-/-}$ peripheral blood donor chimerism at 4 weeks and 45% at 16 weeks, compared with WT donor bone marrow (Figures 2G and 2H). Taken together, our results demonstrate a pervasive developmental defect in *Fancd2*-deficient mice, with a constitutive loss of proliferative capacity and HSC self-renewal that coincides with physiological replication stress during developmental expansion in the FL.

Fancd2$^{-/-}$ FL HSPCs Show Activated DNA-Damage Responses and Accumulation of DNA Strand Breaks

Hypothesizing that the DNA replication stress during rapid cell division in FL HSPCs requires FA pathway integrity, we investigated whether DNA-damage response (DDR) elements were activated in *Fancd2*$^{-/-}$ FL at 14.5 dpc. We assessed the presence of spontaneous double-strand breaks by conducting immunofluorescent labeling of γH2AX in SCA1-enriched FL HSPCs. Although *Fancd2*$^{-/-}$ FL HSPCs showed a modest increase in the percentage of cells presenting more than five γH2AX foci, no statistical difference between WT and *Fancd2*$^{-/-}$ FL HSPCs was observed at lower levels of damage (Figures 3A and 3B). As a validated alternative, we then sought evidence of DNA repair activation by investigating the presence of nuclear RAD51, a protein that binds single-stranded DNA to facilitate homologous strand searching (Lundin et al., 2003), and observed a significant increase in the percentage of HSPCs with RAD51 foci in *Fancd2*$^{-/-}$ FL, compared with WT (Figures 3C and 3D). Next, we assayed the relative expression of DDR genes in *Fancd2*$^{-/-}$ and WT FL HSPC. Among SCA1^{+} FL cells, we found a consistent trend for transcriptional upregulation of genes involved in both HR and NHEJ, including *Rad51*, *Xrcc5*, *Xrcc6*, *Xrcc2*, and *Prkdc*, in *Fancd2*$^{-/-}$, although only Prkdc was statistically significant (Figure 3E). In an additional survey of *Rad51*, *Xrcc2*, and *Prkdc* transcripts in the more highly enriched ASL HSPC population, we found that *Xrcc2* was significantly upregulated, with *Rad51* expression trending upward in *Fancd2*-deficient cells (Figure 3F). Finally, we sought to corroborate DNA damage in *Fancc*$^{-/-}$ and *Fancd2*$^{-/-}$ FL HSPCs via the alkaline comet assay, a measure of single- or double-strand breaks (Beerman et al., 2014). Analysis of SCA1-enriched FL HSPCs showed a significant increase in strand breaks in both *Fancc*$^{-/-}$ and *Fancd2*$^{-/-}$ FL compared with WT (Figures 3G–3I). Importantly, cells assayed were not subjected to exogenous stress via interstrand crosslinker exposure. Thus, the aggregate results demonstrate a broad DDR in response to fetal hematopoietic replicative demand in the context of FA pathway deficiency.

Fancd2$^{-/-}$ FL HSPCs Exhibit Constitutive Activation of p53-Independent Downstream Stress Responders

Adult FA HSPCs undergo apoptosis and exhibit a canonical p53 response elicited by exogenous cell stress (Ceccaldi et al., 2012). Similarly, under exogenous induction such as irradiation, p53 is phosphorylated in both WT and *Fancd2*$^{-/-}$ SCA1^{+} FL cells (Figure 4A). However, in our analyses of total and phosphorylated (Ser15) p53 expression in unperturbed fetal HSPCs, by western blot and phosphoflow cytometry, respectively, we found no major difference between WT and *Fancd2*$^{-/-}$ FL cells (Figures 4B–4E). Consistent with this apparent lack of p53 response, we found no evidence of apoptosis in *Fancd2*$^{-/-}$ HSPCs when we analyzed annexin V staining by flow cytometry and expression of pro-apoptotic p53 target genes, *Puma* and *Noxa* (Figures 4F and 4G). During the cell-cycle analysis using Ki-67 and Hoechst staining (Figure 4H), we observed the rapid cell-cycling characteristics of FL with ~90% of KSL cells out of the quiescent state. However, there was neither checkpoint arrest nor a significant difference in the proportion of cells in each cell-cycle state between WT and *Fancd2*$^{-/-}$ (Figure 4I). To further delineate the canonical stress response, we next studied the expression of phosphorylated ataxia telangiectasia mutated (ATM), an upstream kinase of DDR and cell-cycle

(D) Schema for FL transplantation into primary and secondary recipients. For the primary, each FL donor was transplanted into three recipients (donor n = 2 WT and 4 KO FLs from two litters). In the subsequent transplantation, bone marrow from two WT to three KO primary recipients were injected into three recipients per donor.
(E) CD45.2 chimerism in peripheral blood of primary recipients at 4 weeks ($p = 0.02$) and 14 weeks ($p = 0.006$) post transplant.
(F) CD45.2 chimerism in peripheral blood of secondary recipients at 4 weeks ($p < 0.001$) and 14 weeks ($p = 0.02$) post transplant.
(G) Transplantation schema for adult bone marrow cells. Each donor was transplanted into five recipients (donor n = 2 WT and 2 KO).
(H) CD45.2 chimerism in peripheral blood ($p < 0.001$ at both time points).
Error bars reflect SEM, and asterisks indicate *$p \leq 0.05$, **$p \leq 0.01$, and ***$p \leq 0.001$.

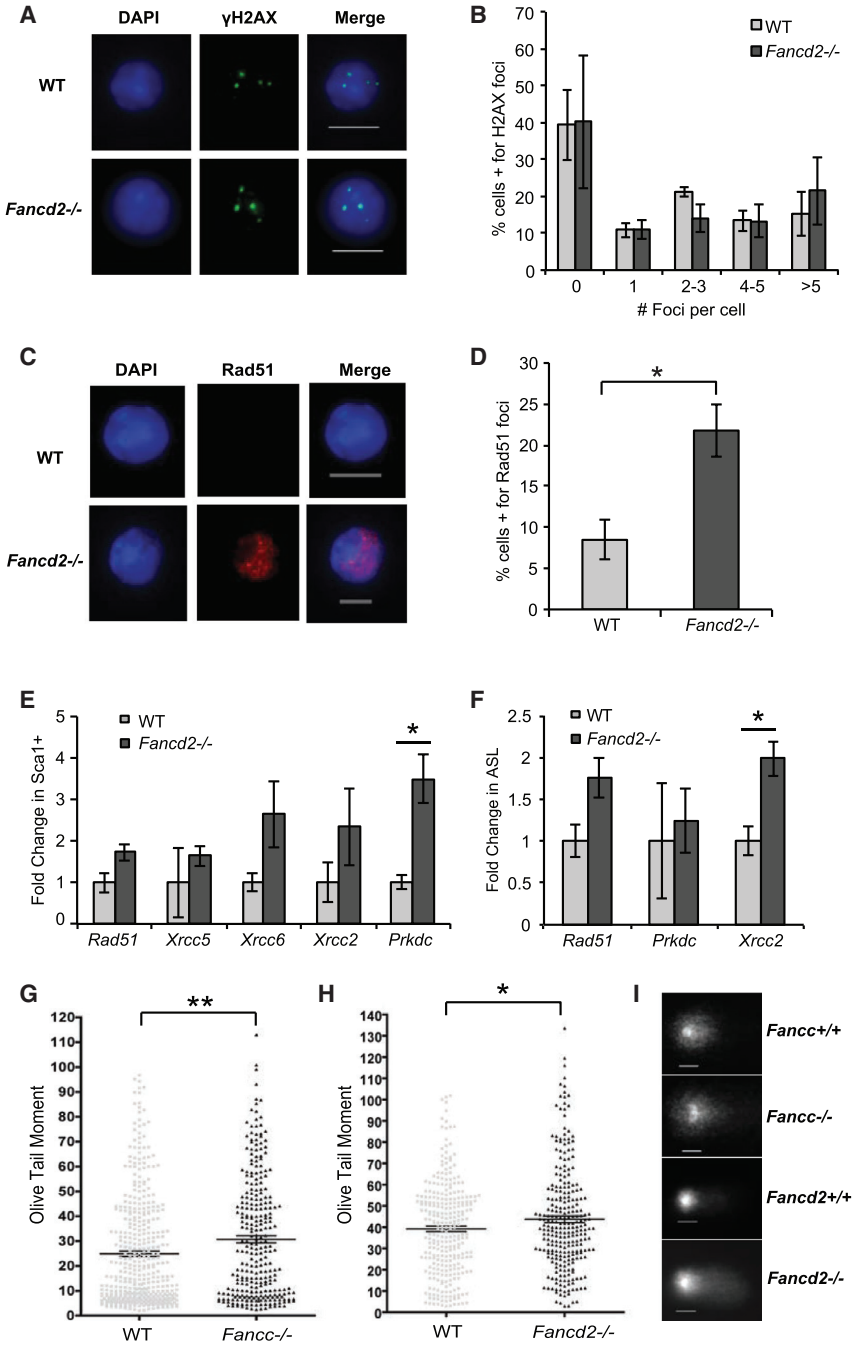

Figure 3. DNA-Damage Responses Are Induced, and the Strand Breaks Are Accumulated in FA FL HSPCs

(A) Representative γH2AX foci in SCA1$^+$ FL cells (60× objective lens; the scale bar represents 5 μm).

(B) Quantification of γH2AX foci per cell (n = 3 WT and 3 KO from three litters).

(C) Representative RAD51 foci in SCA1$^+$ FL (60× objective lens; the scale bar represents 5 μm).

(D) Quantification of cells positive for foci ($p = 0.02$, n = 6 WT and 6 KO from three litters).

(E) Expression of DDR genes in SCA1$^+$ FL cells ($p = 0.08$, 0.44, 0.06, 0.22, and 0.005, respectively; n = 4 WT and 4 KO from three litters).

(F) Expression of selected DDR genes in ASL-sorted FL cells ($p = 0.08$, 0.5, 0.04 respectively; n = 3 WT and 3 KO from two litters).

(G) Olive tail moment of 428 SCA1$^+$ FL cells from seven WT animals and 288 SCA1$^+$ FL cells from five *Fancc*$^{-/-}$ animals from four litters ($p = 0.003$).

(H) Olive tail moment of 289 SCA1$^+$ FL cells from five WT animals and 267 SCA1$^+$ FL cells from five *Fancd2*$^{-/-}$ animals from four litters ($p = 0.04$).

(I) Representative alkaline comets of SCA1$^+$ FL cells (20× objective lens; the scale bar represents 20 μm).

Error bars reflect SEM, and asterisks indicate *$p \leq 0.05$ and **$p \leq 0.01$.

checkpoint (Burma et al., 2001; Ito et al., 2004), by intracellular flow cytometry. In every set of litters we investigated, phospho-ATM was significantly upregulated in *Fancd2*$^{-/-}$ FL compared with WT FL by 24% on average (Figures 4J and 4K). Collectively, our findings elucidate a model of compromised proliferation in *Fancd2*$^{-/-}$ FL HSPC without p53-mediated cell-cycle arrest or apoptosis in response to replication stress.

Fancd2$^{-/-}$ FL Progenitor and Repopulating Defects Are Partially Reversed by p38 MAPK Inhibition

Because the experimental induction of cell stress in FA hematopoietic cells prompts expression of p38 mitogen-activated protein kinase (MAPK), which senses DNA damage and maintains HSPC proliferation and self-renewal (Ito et al., 2004; Saadatzadeh et al., 2009; Svahn et al., 2015), we asked whether *Fancd2*$^{-/-}$ FL HSPCs also show increased

p38 MAPK activation during rapid FL expansion. Here, we used intracellular flow cytometry and immunofluorescence assays (Figures 5A and 5B) and found significant constitutive activation of p38 MAPK in *Fancd2*$^{-/-}$ FL compared with WT FL from both methods (Figures 5C and 5D). We then sought to determine whether p38 MAPK inhibition would rescue proliferation in *Fancd2*$^{-/-}$ FL HSPCs. First, we investigated hematopoietic output via colony formation in methylcellulose, with and without the addition of the p38 MAPK inhibitors SB203580 and LY2228820. Co-culture with 10 μM SB203580 and 100 nM LY2228820 significantly increased colony formation from *Fancd2*$^{-/-}$ FL progenitors by 120%, eliminating the difference in colony formation between WT and *Fancd2*$^{-/-}$ (Figure 5E). Next, we cultured unfractionated *Fancd2*$^{-/-}$ and WT FL cells overnight with 10 μM SB203580 or DMSO vehicle control and transplanted them into sublethally irradiated congenic recipient mice. Subsequently, we injected mice with SB203580 or DMSO intraperitoneally, three times weekly, as previously described (Ito et al., 2006) (Figure 5F). Strikingly, in vivo inhibition of p38 MAPK significantly improved the repopulation of *Fancd2*$^{-/-}$ FL at the week 4 time point, when engraftment was on a par with WT control recipients (Figure 5G). At a later time point (week 11), donor chimerism remained similar to that of the early time point. However, statistical significance was lost due to animal deaths potentially caused by the susceptibility of *Fancd2*$^{-/-}$ FL recipients to the toxicity of DMSO (Figure 5F). Altogether, our data demonstrate activation of a canonical cell stress pathway in *Fancd2*$^{-/-}$ FL that is amenable to pharmacological rescue.

DISCUSSION

HSPC function under stress conditions is severely compromised in models with experimentally disabled DDR (Beerman et al., 2014), and our data indicate that DNA repair integrity via the FA pathway is required for proper HSPC pool expansion during development. Mechanistically, HSPC depletion in the FL differs from progressive postnatal losses after exposure to exogenous alkylating agents, aldehyde metabolites, or innate immunostimulation (Garaycoechea and Patel, 2014; Hu et al., 2013; Kutler et al., 2003; Pontel et al., 2015; Walter et al., 2015). Accordingly, the moderately severe spontaneous hematopoietic defects observed in *Fancd2* adult mice (Parmar et al., 2010; Zhang et al., 2010) and in FA patients would represent postnatal progression of hematopoietic failure rather than a de novo onset (Auerbach et al., 1990; Ceccaldi et al., 2012).

During hematopoietic development in the FL, rapidly cycling HSPCs experience significant replicative stress (Fleming et al., 1993; Mikkola and Orkin, 2006; Morrison et al., 1995; Morrison and Spradling, 2008). DNA repair integrity is crucial in mitigating replication stress during HSPC pool expansion and maintenance of genome stability (Alvarez et al., 2015; Bakker and Passegue, 2013; Beerman et al., 2014; Zhang et al., 2011). Our data comparing phenotypes and progenitor frequency of FL HSPCs between 12.5 and 14.5 dpc provide evidence that *Fancd2*-deficient HSPCs fail to adequately expand in the fetal liver, coincident with DNA-damage accumulation and elevated stress response observed at 14.5 dpc. Equivalent ASL and SLAM frequencies, as well as the colony formation by WT and *Fancd2*$^{-/-}$ HSPCs at 12.5 dpc, indeed suggest that the significant hematopoietic attrition occurs during FL expansion, a narrow time period of heightened replicative demand. At 14.5 dpc, we confirm significant SLAM-HSC deficits and dramatically diminished proliferative capacity during *Fancd2* deficiency, thereby setting the stage for postnatal *Fancd2*$^{-/-}$ bone marrow HSPC compromise.

The ensuing replication stress during rapid expansion elicits a broad DDR, when *Fancd2*$^{-/-}$-deficient HSPC accumulate DNA damage and activate p38 MAPK in response to physiological replication demands encountered during development. The lack of a more robust γH2AX phosphorylation seemed initially surprising to us, but has been reported before (Burma et al., 2001; Ciccia and Elledge, 2010; Zha et al., 2008). However, a significant accumulation of DNA strand breaks, as well as RAD51 foci, along with the transcriptional elevation of repair genes in the ASL-sorted population clearly indicate the overall activation of DDR in *Fancd2*$^{-/-}$ HSPCs (Beerman et al., 2014; Mohrin et al., 2010; Zhang et al., 2016). Not surprisingly, the magnitude of DDR was comparatively more modest in *Fancd2*$^{-/-}$ FL HSPCs than that observed after typical interstrand crosslinker exposure or chronic injury models (Hu et al., 2013; Walter et al., 2015). This is entirely consistent with an operational model of diminished, but not eliminated in utero HSPC function, and experimentally supported by fetal deficits in *Fancd2*$^{-/-}$ that are not due to apoptosis but rather result from diminished proliferative capacity (Alvarez et al., 2015; Shen et al., 2013; Zhang et al., 2011). Our observations are further consistent with spontaneous developmental deficits that arise during rapid mitotic cycles in *Fancc* and *Fancm* germ cell proliferation (Luo et al., 2014; Nadler and Braun, 2000).

Fetal HSPCs display unique molecular and functional properties before they transition postnatally to the definitive adult phenotype (Bowie et al., 2007). Although p53 is readily phosphorylated by irradiation in both WT and *Fancd2*$^{-/-}$ FL HSPCs and active during development in general (reviewed in Molchadsky et al., 2010), our studies reveal that fetal FA HSPC DDRs are independent of p53 activation. This finding diverges from a well-described phenotype in adult FA models (Ceccaldi et al., 2012; Garaycoechea and Patel, 2014; Zhang et al., 2013). A recent study

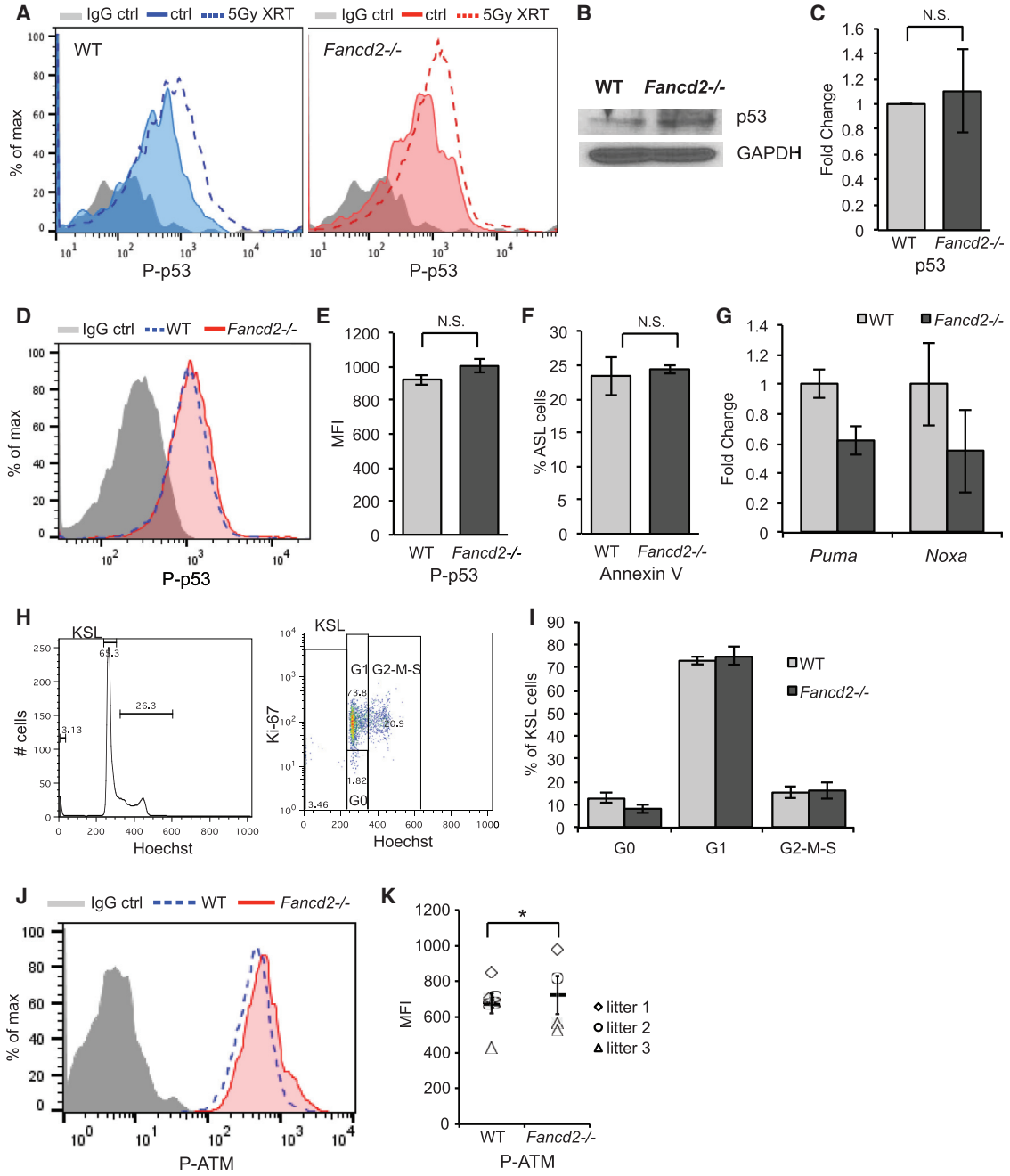

Figure 4. FA Fetal HSPC Attrition Is Not Associated with p53-Mediated Apoptosis or Cell-Cycle Arrest

(A) Representative histogram showing the activation of phospho-p53 (ser15) after 5 Gy irradiation in WT and *Fancd2*$^{-/-}$ FL, respectively, compared with the non-irradiated controls.

(B) Immunoblots for p53 and GAPDH from whole FL lysates (bands are representative of multiple experiments, n = 3).

(C) Densitometry of p53 protein bands from *Fancd2*$^{-/-}$ whole FL compared with WT, normalized to GAPDH (p = 0.78, n = 7 WT and 4 KO from 3 litters).

(D) Representative histogram showing the intracellular staining of phospho-p53 (ser15) in WT and *Fancd2*$^{-/-}$ SCA1^{+} FL cells.

(E) Expression of phospho-p53 (ser15) in WT and *Fancd2*$^{-/-}$ SCA1^{+} FL cells as the mean frequency of intensity (p = 0.16, n = 5 WT and 3 KO from two litters).

(F) Percentage of ASL cells positive for annexin V (p = 0.75, n = 5 WT and 5 KO from two litters).

(legend continued on next page)

shows that the p53 response is indeed linearly correlated with the number of DNA breaks (Loewer et al., 2013). Hence, it is conceivable FL HSPCs at 14.5 dpc may not have accumulated enough DNA damage to reach threshold p53 activity to induce apoptosis or cell-cycle arrest. The data consistently show that *Fancd2*$^{-/-}$ FL cells encounter genomic stress that activates DDR elements during replication, not seen in adult HSPCs (Fleming et al., 1993). Similar to a previous report on HSPC development (Nygren et al., 2006), we find no accumulation in G_0, G_1, or S-G_2-M cell-cycle phase, suggesting that cell-cycle transit is evenly prolonged, whereby ATM activation is insufficient to activate checkpoints, leaving cell-cycle phase distribution unchanged, even as *Fancd2*$^{-/-}$ proliferation and repopulation decline.

Others showed that constitutive activation of the p38 MAPK "stress kinase" results in HSPC pool depletion (Bakker and Passegue, 2013; Ito et al., 2006). Our studies herein not only corroborate activation of p38 MAPK in *Fancd2*$^{-/-}$ FL cells, but demonstrate rescue of the proliferative capacity after pharmacological p38 MAPK inhibition both in vitro and in vivo (Ito et al., 2004, 2006). Although our in vivo treatment with SB203580 in *Fancd2*$^{-/-}$ FL recipients precluded full evaluation of the long-term effect on HSCs, rescue strategies involving short-term p38 MAPK inhibition or using a more potent and less toxic compound, such as LY2228820 (Campbell et al., 2014), might provide a more definitive answer. Yet while several reports and our data imply that p38 MAPK could be a potential therapeutic target to ameliorate hematopoietic failure in FA patients, it is important to consider that this leaves HSPCs vulnerable to DNA-damage accumulation and genomic instability (Anur et al., 2012; Briot et al., 2008; Garbati et al., 2013; Pearl-Yafe et al., 2004; Saadatzadeh et al., 2009).

Taken together, we demonstrate that *Fancd2*$^{-/-}$ mice exhibit a pervasive developmental HSPC defect that echoes the constitutional defects evident at birth in a subset of FA patients. Mechanistically, the data support a model whereby the physiological replication stress in rapidly cycling *Fancd2*$^{-/-}$ fetal HSPCs spontaneously elicits DNA damage and promotes the activation of p38 MAPK, resulting a diminished proliferative fitness, but without the characteristic postnatal p53-mediated apoptotic response.

EXPERIMENTAL PROCEDURES

Mice

Mice were handled in accordance with OHSU IACUC guidelines. FLs were harvested at 12.5 and 14.5 dpc during timed pregnancies (vaginal plug method) from C57BL/6 *Fancd2*$^{+/-}$ dams (Houghtaling et al., 2003). Fetal tissues were genotyped using the Phire PCR Kit (Thermo Scientific). Bone marrow cells from adult animals were harvested as previously described (Skinner et al., 2008).

CFU-c

Methylcellulose progenitor assays (Mouse Methylcellulose Complete Media, R&D Systems) were performed according to the manufacturer's instructions with unfractionated FL cells plated at a concentration of 20,000 cells/mL. Assays with p38 MAPK inhibition were conducted with 10 μM SB203580 (Calbiochem), 100 nM LY2228820 (Selleckchem), or DMSO vehicle control.

Transplantation

Fetal liver transplants were performed with unfractionated FL cells (8×10^5) by tail-vein injection into sublethally irradiated (750 cGy) congenic CD45.1 recipients. Transplantation assays with in vivo p38 MAPK inhibition were conducted after overnight incubation of unfractionated FL cells with either 10 μM SB203580 (Calbiochem) or DMSO vehicle control; cells were then washed and injected into irradiated recipients. Recipients received either 15 mg/kg SB203580 or DMSO via intraperitoneal injection three times per week as previously described (Ito et al., 2006). For adult bone marrow transplants, 1×10^6 whole bone marrow cells were transplanted into irradiated (750 cGy) CD45.1 recipients. Chimerism analysis was as previously described (Skinner et al., 2008).

Flow Cytometry

For the KSL, ASL, and SLAM HSPC analyses, single-cell suspended $2–4 \times 10^6$ whole FL cells were washed in fluorescence-activated cell sorting (FACS) buffer (Dulbecco's PBS, 2% fetal bovine serum [FBS]) and stained using LIVE/DEAD Fixable Green (Thermo Scientific L23101), cKIT (BioLegend 105819), SCA1 (eBioscience 25-5981-81), AA4.1/CD93 (eBioscience 17-5892-82), CD48 (BioLegend 103422), and CD150 (BioLegend 115925) antibodies, as well as the lineage antibodies: B220 (BD 553090), GR1 (BioLegend 108408), CD3 (BD 555275), CD4 (BD 553653), CD5 (BD 553023), and TER119 (BD 553673) at the manufacturers' recommended concentrations (excluding MAC1 in FL analyses [Morrison et al., 1995]). For the cell-cycle analysis, cells were stained for the populations above as well as 20 μL fluorescein isothiocyanate anti-Ki-67 or anti-mouse immunoglobulin G1 (IgG1) (BD 556026) and 0.1 μg/ml Hoechst

(G) Expression of *Puma* and *Noxa* in WT and *Fancd2*$^{-/-}$ ASL FL cells by real-time qPCR ($p = 0.02$ and 0.16, respectively; n = 3 WT and 3 KO from two litters).
(H) Representative histogram and dot plot demonstrating Hoechst and Ki-67 staining for the cell-cycle analysis of *Fancd2*$^{-/-}$ KSL FL.
(I) Comparison between WT and *Fancd2*$^{-/-}$ FL KSL cells in G_0, G_1, and G_2-M-S phases of the cell cycle (n = 11 WT, 8 KO from four litters).
(J) Representative histogram showing the intracellular staining of phospho-ATM (Ser1981) in WT and *Fancd2*$^{-/-}$ KSL FL cells.
(K) Expression of phospho-ATM (Ser1981) in WT and *Fancd2*$^{-/-}$ KSL FL cells as the mean frequency of intensity ($p = 0.03$, data were paired by the litter for t test; n = 2 WT, 1 KO in litter 1; n = 3 WT, 1 KO in litter 2; n = 1 WT, 2 KO in litter 3).
Error bars reflect SEM and asterisks indicate $^*p \leq 0.05$. N.S., not significant.

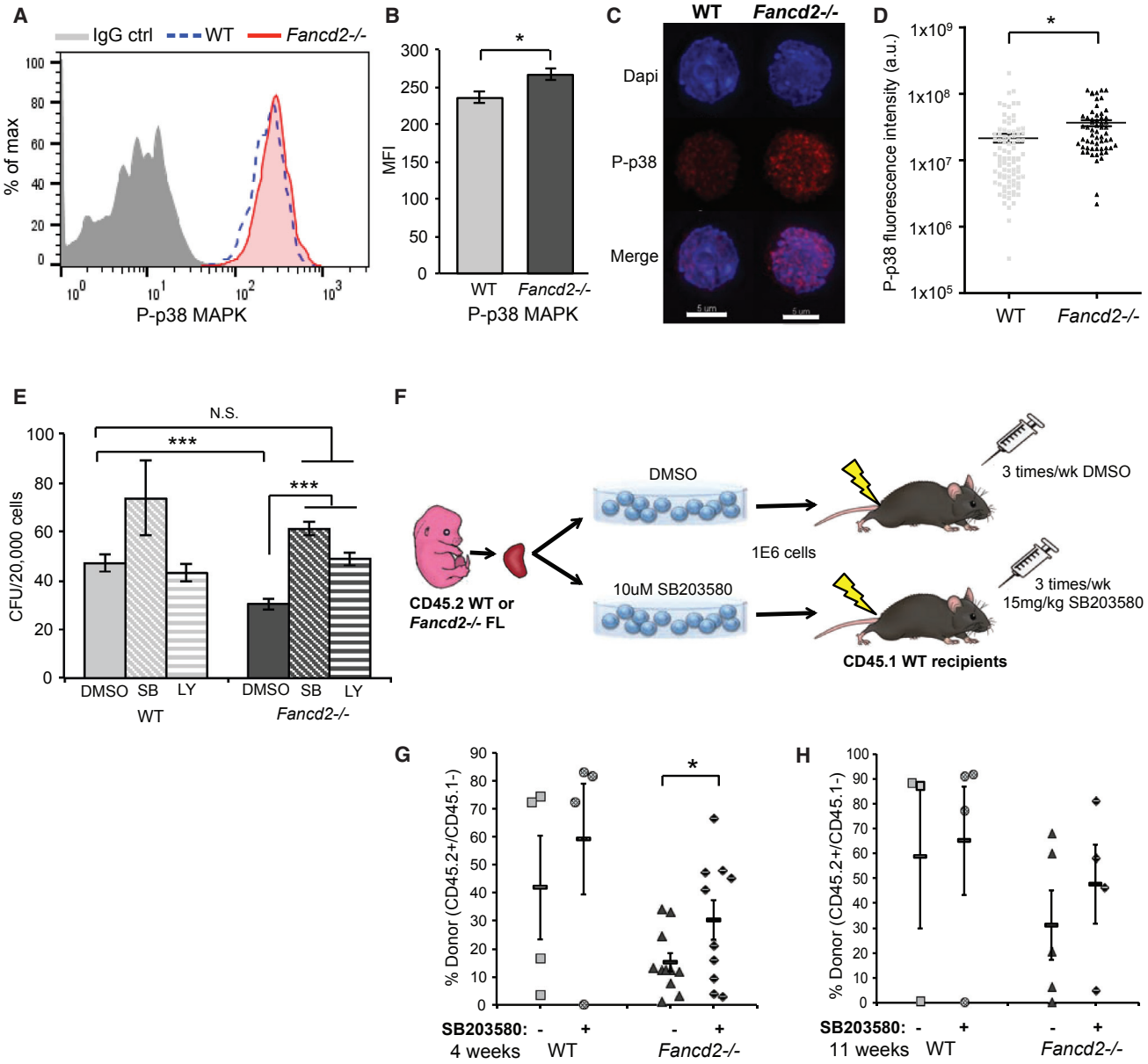

Figure 5. Inhibiting Constitutively Activated p38 MAPK Increases Clonogenicity in *Fancd2*$^{-/-}$ FL

(A) Representative histogram showing the intracellular staining of phospho-p38 MAPK (T180/Y182) in WT and *Fancd2*$^{-/-}$ KSL FL cells.

(B) Expression of phospho-p38 MAPK (T180/Y182) in WT and *Fancd2*$^{-/-}$ KSL FL cells as the mean frequency of intensity ($p = 0.03$, $n = 4$ WT and 4 KO from two litters).

(C) Representative images showing the immunofluorescence staining of phospho-p38 MAPK (T180/Y182) in WT and *Fancd2*$^{-/-}$ SCA1^{+} FL cells (60× objective lens; the scale bar represents 5 μm).

(D) Immunofluorescence intensity of phospho-p38 MAPK (T180/Y182) in WT and *Fancd2*$^{-/-}$ SCA1^{+} FL cells ($p = 0.003$, $n = 5$ WT and 4 KO from three litters).

(E) WT and *Fancd2*$^{-/-}$ colony-forming hematopoietic progenitor cell frequency with and without p38 MAPK inhibitors, 10 μM SB203580, and 100 nM LY2228820 ($p \leq 0.001$ between WT and *Fancd2*$^{-/-}$ at baseline with DMSO, $p \leq 0.001$ between *Fancd2*$^{-/-}$ baseline and both inhibitor conditions, $n = 4$–10 FL per condition from nine litters).

(F) Schema for transplantation of FL cells and p38 MAPK inhibitor treatment.

(legend continued on next page)

(Thermo Scientific 62249). For annexin V staining, cells were stained for ASL, 5 μL annexin V (BioLegend 640906), and 1 μg/mL propidium iodide (Molecular Probes P3566) in ANNEXIN binding buffer (10 mM HEPES, 140 mM NaCl, and 2.5 mM $CaCl_2$ [pH 7.4]). For intracellular staining, KSL stained cells were fixed with 2% paraformaldehyde (PFA), permeabilized with 0.5% saponin, and stained using 0.2 μg PE anti-phospho-ATM (Ser1981) (BioLegend 651203) and 0.2 μg PE rat anti-mouse IgG (BioLegend 406607), or 0.125 μg APC anti-phospho-p38 MAPK (T180/Y182) (eBioscience 17-9078-42) and 0.5 μg APC goat anti-mouse IgG2 (BD 340473), or 1 μg anti-phospho-p53 (Ser15) (Cell Signaling 12571) and 1 μg PE rat anti-rabbit IgG (eBioscience 12-4739-81). Data were collected on a BD FACSCalibur, Canto II, LSR II, or InFlux (BD Biosciences), and analyzed by FlowJo software (TreeStar), using unstained FL cells as the negative controls for gating and anti-IgG-stained cells to normalize the mean fluorescence intensity.

Real-Time qPCR

KSL bone marrow or ASL FL cells were sorted by FACS on BD InFlux. $SCA1^+$ cells were isolated from bone marrow and FL using the Mouse PE Selection Kit (STEMCELL Technologies) with PE anti-SCA1 (BD 553336), and placed in Qiazol. Total RNA was purified with the miRNeasy Mini Kit (Qiagen). mRNA was converted to cDNA using SuperScript III First Strand (Invitrogen). Real-time qPCR was performed on StepOne Plus using Power SYBR Green Master Mix (Applied Biosystems). Primer sequences are described in Table S1. *Fancd2*$^{-/-}$ and WT samples were normalized to *β-actin*, and *Fancd2*$^{-/-}$ gene expression was compared with WT.

Immunofluorescence

Single-cell suspensions of FL were enriched by immunomagnetic selection for SCA1, as for real-time qPCR. Enriched FL HSPCs were fixed in 2% PFA and cytospun onto slides. Cells were permeabilized with NET buffer with 0.5% Triton X-100 (Enns et al., 2012) and stained with Hoechst (Thermo Scientific 62249) and AF488-conjugated anti-γH2AX (BioLegend, 613407), rabbit anti-mouse RAD51 (Santa Cruz Biotechnology, 8349) followed by Cy3 goat anti-rabbit IgG (Millipore, AP132C) or Cy5-conjugated anti-phospho-p38 (T180/Y182) (eBioscience, 17-9078-42). For γH2AX and RAD51 immunofluorescence, cells were imaged using the Zeiss ApoTome system and images were processed with Zen software (Zeiss). For phospho-p38 immunofluorescence, z-stack images were acquired using the DeltaVision Applied Precision System (GE Healthcare), and the fluorescence intensity of cy5 within the nucleus area of each cell was analyzed with Imaris software (Bitplane).

Comet Assay

FL cells were immunomagnetically enriched for SCA1 and then prepared for alkaline comet assay as previously described (Olive and Banath, 2006). Agarose-embedded cells were lysed in alkaline conditions overnight at 4°C followed by electrophoresis. Slides were stained with 2.5 μg/mL propidium iodide, imaged on a Zeiss Axioskop 2 Plus microscope, and analyzed with CaspLab software (Końca et al., 2003).

Western Blot

FL cells were lysed using RIPA buffer with protease and phosphatase inhibitor cocktail (Thermo Scientific), followed by ultrasonication (Cole Parmer CPX-130). Lysates were prepared in LDS sample buffer (Life Technologies) with 10% β-mercaptoethanol and boiled for 5 min for denaturation. Denatured protein lysates were loaded on 4%–15% Tris-HCl PAGE gel (Bio-Rad) for gel electrophoresis separation (50 min at 200 V) and transfer (overnight at 25 V). Transferred membranes were blocked with 5% non-fat dry milk (Carnation, Nestlé) in Tris-buffered saline with Tween 20 and blotted with anti-GAPDH (1:5,000, Novus Biologicals) and anti-p53 (1:500, Santa Cruz), followed by anti-mouse and anti-rabbit IgG horseradish peroxidase conjugates (Promega). Blots were developed on X-ray film after 5-min exposure to the SuperSignal West Pico Chemiluminescent HRP substrate (Thermo Scientific). For quantification, protein band intensities were analyzed using Image Studio Lite 5.2 (LI-COR).

Luminex Cytokine Profiling

FACS-sorted ASL FL cells were cultured in a 96-well plate in HSC medium (Iscove's modified Dulbecco's medium, 15% FBS, 1% penicillin-streptomycin) for 24 hr, and the supernatants were analyzed for cytokines using a mouse Th1/Th2 Luminex panel (eBioscience) which included IL-12, granulocyte macrophage colony-stimulating macrophage (GM-CSF), interferon-γ (IFN-γ), IL-1β, IL-13, IL-18, IL-2, IL-4, IL-5, IL-6, and tumor necrosis factor α (TNF-α). This analysis was performed by the Endocrine Technologies Support Core at the Oregon National Primate Research Center using the manufacturer's instructions. In brief, 25 μL cell-culture supernatant was incubated overnight with antibody-coated, fluorescent-dyed capture microspheres specific for each analyte, followed by detection antibodies and streptavidin-phycoerythrin. Washed microspheres with bound analytes were resuspended in reading buffer and analyzed on a Milliplex Analyzer (EMD Millipore) bead sorter with XPonent Software version 3.1 (Luminex). Data were calculated using Milliplex Analyst software version 5.1 (EMD Millipore). Intra-assay coefficients of variation were as follows: IL-1β, 14.2%; IL-2, 10.4%; IL-4, 6.9%; IL-5, 18.1%; IL-6, 5.7%; IL-13, 7.2%; IFN-γ, 25.4%; IL-12, 14.0%; GM-CSF, 24.5%; TNF-α, 3.8%; IL-18, 6.4%. Because all samples were analyzed in a single assay, no inter-assay variation was calculated.

Statistical Analysis

All numerical results shown are expressed as mean ± SEM. Two-tailed Student's t tests were performed for statistical analyses,

(G) CD45.2 chimerism in peripheral blood of FL recipients with or without SB203580 treatment at 4 weeks post transplant ($p = 0.03$, one-tailed t test between DMSO- and SB-treated *Fancd2*$^{-/-}$ recipients; n = 4 WT + DMSO, 4 WT + SB, 11 KO + DMSO, 10 KO + SB).
(H) CD45.2 chimerism in peripheral blood of FL recipients with or without SB203580 treatment at 11 weeks post transplant (n = 3 WT + DMSO, 4 WT + SB 5 KO + DMSO, 4 KO + SB).
Error bars reflect SEM, and asterisks indicate *$p \leq 0.05$ and ***$p \leq 0.001$. N.S., not significant.

unless otherwise stated in the figure legends. A p value of less than or equal to 0.05 was considered significant.

SUPPLEMENTAL INFORMATION

Supplemental Information includes one table and can be found with this article online at http://dx.doi.org/10.1016/j.stemcr.2016.09.005.

AUTHOR CONTRIBUTIONS

K.J.S., A.N.K.-L., Y.Y., and P.K. designed the study, interpreted the data, and prepared the manuscript. K.J.S., A.N.K.-L., Y.Y., and N.A.G. performed the experiments.

ACKNOWLEDGMENTS

The authors thank Matthew Deater and the Grompe laboratory for supplying C57BL/6 *Fancd2*$^{+/-}$ mice and antibodies, and Michael Garbati for the advice on LY2228820. We are indebted to members of the Flow Cytometry Core Laboratory at OHSU and Nofar Movshovich for assistance with imaging analyses. K.J.S. was supported by the Medical Research Foundation of Oregon Early Clinical Investigator Grant, and A.N.K. was supported by the T32 Molecular Hematology Training Grant. The Endocrine Technologies Support Core (ETSC) at the Oregon National Primate Research Center (ONPRC) is supported by NIH Grant P51 OD011092 awarded to ONPRC. Aspects of this work were presented in part at the American Society of Hematology 55th Annual Meeting in New Orleans, LA, American Society of Hematology 57th Annual Meeting in Orlando, FL, and the American Society of Pediatric Hematology Oncology 27th Annual Meeting in Chicago, IL.

Received: February 23, 2016
Revised: September 8, 2016
Accepted: September 9, 2016
Published: October 6, 2016

REFERENCES

Alvarez, S., Diaz, M., Flach, J., Rodriguez-Acebes, S., Lopez-Contreras, A.J., Martinez, D., Canamero, M., Fernandez-Capetillo, O., Isern, J., Passegue, E., et al. (2015). Replication stress caused by low MCM expression limits fetal erythropoiesis and hematopoietic stem cell functionality. Nat. Commun. *6*, 8548.

Anur, P., Yates, J., Garbati, M.R., Vanderwerf, S., Keeble, W., Rathbun, K., Hays, L.E., Tyner, J.W., Svahn, J., Cappelli, E., et al. (2012). p38 MAPK inhibition suppresses the TLR-hypersensitive phenotype in FANCC- and FANCA-deficient mononuclear phagocytes. Blood *119*, 1992–2002.

Auerbach, A.D., Liu, Q., Ghosh, R., Pollack, M.S., Douglas, G.W., and Broxmeyer, H.E. (1990). Prenatal identification of potential donors for umbilical cord blood transplantation for Fanconi anemia. Transfusion *30*, 682–687.

Bakker, S.T., and Passegue, E. (2013). Resilient and resourceful: genome maintenance strategies in hematopoietic stem cells. Exp. Hematol. *41*, 915–923.

Beerman, I., Seita, J., Inlay, M.A., Weissman, I.L., and Rossi, D.J. (2014). Quiescent hematopoietic stem cells accumulate DNA damage during aging that is repaired upon entry into cell cycle. Cell Stem Cell *15*, 37–50.

Bowie, M.B., Kent, D.G., Dykstra, B., McKnight, K.D., McCaffrey, L., Hoodless, P.A., and Eaves, C.J. (2007). Identification of a new intrinsically timed developmental checkpoint that reprograms key hematopoietic stem cell properties. Proc. Natl. Acad. Sci. USA *104*, 5878–5882.

Briot, D., Mace-Aime, G., Subra, F., and Rosselli, F. (2008). Aberrant activation of stress-response pathways leads to TNF-alpha oversecretion in Fanconi anemia. Blood *111*, 1913–1923.

Burma, S., Chen, B.P., Murphy, M., Kurimasa, A., and Chen, D.J. (2001). ATM phosphorylates histone H2AX in response to DNA double-strand breaks. J. Biol. Chem. *276*, 42462–42467.

Campbell, R.M., Anderson, B.D., Brooks, N.A., Brooks, H.B., Chan, E.M., De Dios, A., Gilmour, R., Graff, J.R., Jambrina, E., Mader, M., et al. (2014). Characterization of LY2228820 dimesylate, a potent and selective inhibitor of p38 MAPK with antitumor activity. Mol. Cancer Ther. *13*, 364–374.

Ceccaldi, R., Parmar, K., Mouly, E., Delord, M., Kim, J.M., Regairaz, M., Pla, M., Vasquez, N., Zhang, Q.S., Pondarre, C., et al. (2012). Bone marrow failure in Fanconi anemia is triggered by an exacerbated p53/p21 DNA damage response that impairs hematopoietic stem and progenitor cells. Cell Stem Cell *11*, 36–49.

Ciccia, A., and Elledge, S.J. (2010). The DNA damage response: making it safe to play with knives. Mol. Cell *40*, 179–204.

Copley, M.R., Babovic, S., Benz, C., Knapp, D.J., Beer, P.A., Kent, D.G., Wohrer, S., Treloar, D.Q., Day, C., Rowe, K., et al. (2013). The Lin28b-let-7-Hmga2 axis determines the higher self-renewal potential of fetal haematopoietic stem cells. Nat. Cell Biol. *15*, 916–925.

Ema, H., and Nakauchi, H. (2000). Expansion of hematopoietic stem cells in the developing liver of a mouse embryo. Blood *95*, 2284–2288.

Enns, C.A., Ahmed, R., and Zhang, A.-S. (2012). Neogenin interacts with matriptase-2 to facilitate hemojuvelin cleavage. J. Biol. Chem. *287*, 35104–35117.

Flach, J., Bakker, S.T., Mohrin, M., Conroy, P.C., Pietras, E.M., Reynaud, D., Alvarez, S., Diolaiti, M.E., Ugarte, F., Forsberg, E.C., et al. (2014). Replication stress is a potent driver of functional decline in ageing haematopoietic stem cells. Nature *512*, 198–202.

Fleming, W.H., Alpern, E.J., Uchida, N., Ikuta, K., Spangrude, G.J., and Weissman, I.L. (1993). Functional heterogeneity is associated with the cell cycle status of murine hematopoietic stem cells. J. Cell Biol. *122*, 897–902.

Garaycoechea, J.I., and Patel, K.J. (2014). Why does the bone marrow fail in Fanconi anemia? Blood *123*, 26–34.

Garbati, M.R., Hays, L.E., Keeble, W., Yates, J.E., Rathbun, R.K., and Bagby, G.C. (2013). FANCA and FANCC modulate TLR and p38 MAPK-dependent expression of IL-1beta in macrophages. Blood *122*, 3197–3205.

Grompe, M., and D'Andrea, A. (2001). Fanconi anemia and DNA repair. Hum. Mol. Genet. *10*, 2253–2259.

Houghtaling, S., Timmers, C., Noll, M., Finegold, M.J., Jones, S.N., Meyn, M.S., and Grompe, M. (2003). Epithelial cancer in Fanconi anemia complementation group D2 (Fancd2) knockout mice. Genes Dev. *17*, 2021–2035.

Hu, L., Huang, W., Hjort, E., and Eklund, E.A. (2013). Increased Fanconi C expression contributes to the emergency granulopoiesis response. J. Clin. Invest. *123*, 3952–3966.

Ito, K., Hirao, A., Arai, F., Matsuoka, S., Takubo, K., Hamaguchi, I., Nomiyama, K., Hosokawa, K., Sakurada, K., Nakagata, N., et al. (2004). Regulation of oxidative stress by ATM is required for self-renewal of haematopoietic stem cells. Nature *431*, 997–1002.

Ito, K., Hirao, A., Arai, F., Takubo, K., Matsuoka, S., Miyamoto, K., Ohmura, M., Naka, K., Hosokawa, K., Ikeda, Y., et al. (2006). Reactive oxygen species act through p38 MAPK to limit the lifespan of hematopoietic stem cells. Nat. Med. *12*, 446–451.

Kamimae-Lanning, A.N., Goloviznina, N.A., and Kurre, P. (2013). Fetal origins of hematopoietic failure in a murine model of Fanconi anemia. Blood *121*, 2008–2012.

Kee, Y., and D'Andrea, A.D. (2012). Molecular pathogenesis and clinical management of Fanconi anemia. J. Clin. Invest. *122*, 3799–3806.

Kiel, M.J., Yilmaz, O.H., Iwashita, T., Yilmaz, O.H., Terhorst, C., and Morrison, S.J. (2005). SLAM family receptors distinguish hematopoietic stem and progenitor cells and reveal endothelial niches for stem cells. Cell *121*, 1109–1121.

Kim, I., He, S., Yilmaz, O.H., Kiel, M.J., and Morrison, S.J. (2006). Enhanced purification of fetal liver hematopoietic stem cells using SLAM family receptors. Blood *108*, 737–744.

Knipscheer, P., Raschle, M., Smogorzewska, A., Enoiu, M., Ho, T.V., Scharer, O.D., Elledge, S.J., and Walter, J.C. (2009). The Fanconi anemia pathway promotes replication-dependent DNA interstrand cross-link repair. Science *326*, 1698–1701.

Końca, K., Lankoff, A., Banasik, A., Lisowska, H., Kuszewski, T., Góźdź, S., Koza, Z., and Wojcik, A. (2003). A cross-platform public domain PC image-analysis program for the comet assay. Mutat. Res. *534*, 15–20.

Korthof, E.T., Svahn, J., Peffault de Latour, R., Terranova, P., Moins-Teisserenc, H., Socie, G., Soulier, J., Kok, M., Bredius, R.G., van Tol, M., et al. (2013). Immunological profile of Fanconi anemia: a multicentric retrospective analysis of 61 patients. Am. J. Hematol. *88*, 472–476.

Kottemann, M.C., and Smogorzewska, A. (2013). Fanconi anaemia and the repair of Watson and Crick DNA crosslinks. Nature *493*, 356–363.

Kutler, D.I., Singh, B., Satagopan, J., Batish, S.D., Berwick, M., Giampietro, P.F., Hanenberg, H., and Auerbach, A.D. (2003). A 20-year perspective on the International Fanconi Anemia Registry (IFAR). Blood *101*, 1249–1256.

Lindahl, T. (1993). Instability and decay of the primary structure of DNA. Nature *362*, 709–715.

Loewer, A., Karanam, K., Mock, C., and Lahav, G. (2013). The p53 response in single cells is linearly correlated to the number of DNA breaks without a distinct threshold. BMC Biol. *11*, 114.

Lossaint, G., Larroque, M., Ribeyre, C., Bec, N., Larroque, C., Decaillet, C., Gari, K., and Constantinou, A. (2013). FANCD2 binds MCM proteins and controls replisome function upon activation of s phase checkpoint signaling. Mol. Cell *51*, 678–690.

Luebben, S.W., Kawabata, T., Johnson, C.S., O'Sullivan, M.G., and Shima, N. (2014). A concomitant loss of dormant origins and FANCC exacerbates genome instability by impairing DNA replication fork progression. Nucleic Acids Res. *42*, 5605–5615.

Lundin, C., Schultz, N., Arnaudeau, C., Mohindra, A., Hansen, L.T., and Helleday, T. (2003). RAD51 is involved in repair of damage associated with DNA replication in mammalian cells. J. Mol. Biol. *328*, 521–535.

Luo, Y., Hartford, S.A., Zeng, R., Southard, T.L., Shima, N., and Schimenti, J.C. (2014). Hypersensitivity of primordial germ cells to compromised replication-associated DNA repair involves ATM-p53-p21 signaling. PLoS Genet. *10*, e1004471.

Mikkola, H.K., and Orkin, S.H. (2006). The journey of developing hematopoietic stem cells. Development *133*, 3733–3744.

Mohrin, M., Bourke, E., Alexander, D., Warr, M.R., Barry-Holson, K., Le Beau, M.M., Morrison, C.G., and Passegue, E. (2010). Hematopoietic stem cell quiescence promotes error-prone DNA repair and mutagenesis. Cell Stem Cell *7*, 174–185.

Molchadsky, A., Rivlin, N., Brosh, R., Rotter, V., and Sarig, R. (2010). p53 is balancing development, differentiation and de-differentiation to assure cancer prevention. Carcinogenesis *31*, 1501–1508.

Morrison, S.J., and Spradling, A.C. (2008). Stem cells and niches: mechanisms that promote stem cell maintenance throughout life. Cell *132*, 598–611.

Morrison, S.J., Hemmati, H.D., Wandycz, A.M., and Weissman, I.L. (1995). The purification and characterization of fetal liver hematopoietic stem cells. Proc. Natl. Acad. Sci. USA *92*, 10302–10306.

Nadler, J.J., and Braun, R.E. (2000). Fanconi anemia complementation group C is required for proliferation of murine primordial germ cells. Genesis *27*, 117–123.

Nygren, J.M., Bryder, D., and Jacobsen, S.E. (2006). Prolonged cell cycle transit is a defining and developmentally conserved hemopoietic stem cell property. J. Immunol. *177*, 201–208.

Olive, P.L., and Banath, J.P. (2006). The comet assay: a method to measure DNA damage in individual cells. Nat. Protoc. *1*, 23–29.

Parmar, K., Kim, J., Sykes, S.M., Shimamura, A., Stuckert, P., Zhu, K., Hamilton, A., Deloach, M.K., Kutok, J.L., Akashi, K., et al. (2010). Hematopoietic stem cell defects in mice with deficiency of Fancd2 or Usp1. Stem Cells *28*, 1186–1195.

Pearl-Yafe, M., Halperin, D., Scheuerman, O., and Fabian, I. (2004). The p38 pathway partially mediates caspase-3 activation induced by reactive oxygen species in Fanconi anemia C cells. Biochem. Pharmacol. *67*, 539–546.

Pontel, L.B., Rosado, I.V., Burgos-Barragan, G., Garaycoechea, J.I., Yu, R., Arends, M.J., Chandrasekaran, G., Broecker, V., Wei, W., Liu, L., et al. (2015). Endogenous Formaldehyde is a hematopoietic stem cell genotoxin and metabolic carcinogen. Mol. Cell *60*, 177–188.

Rathbun, R.K., Faulkner, G.R., Ostroski, M.H., Christianson, T.A., Hughes, G., Jones, G., Cahn, R., Maziarz, R., Royle, G., Keeble, W., et al. (1997). Inactivation of the Fanconi anemia group C

gene augments interferon-gamma-induced apoptotic responses in hematopoietic cells. Blood *90*, 974–985.

Saadatzadeh, M.R., Bijangi-Vishehsaraei, K., Kapur, R., and Haneline, L.S. (2009). Distinct roles of stress-activated protein kinases in Fanconi anemia-type C-deficient hematopoiesis. Blood *113*, 2655–2660.

Shen, C., Oswald, D., Phelps, D., Cam, H., Pelloski, C.E., Pang, Q., and Houghton, P.J. (2013). Regulation of FANCD2 by the mTOR pathway contributes to the resistance of cancer cells to DNA double-strand breaks. Cancer Res. *73*, 3393–3401.

Skinner, A.M., O'Neill, S.L., Grompe, M., and Kurre, P. (2008). CXCR4 induction in hematopoietic progenitor cells from Fanca(-/-), -c(-/-), and -d2(-/-) mice. Exp. Hematol. *36*, 273–282.

Svahn, J., Lanza, T., Rathbun, K., Bagby, G., Ravera, S., Corsolini, F., Pistorio, A., Longoni, D., Farruggia, P., Dufour, C., et al. (2015). p38 Mitogen-activated protein kinase inhibition enhances in vitro erythropoiesis of Fanconi anemia, complementation group A-deficient bone marrow cells. Exp. Hematol. *43*, 295–299.

Tulpule, A., Lensch, M.W., Miller, J.D., Austin, K., D'Andrea, A., Schlaeger, T.M., Shimamura, A., and Daley, G.Q. (2010). Knockdown of Fanconi anemia genes in human embryonic stem cells reveals early developmental defects in the hematopoietic lineage. Blood *115*, 3453–3462.

Walter, D., Lier, A., Geiselhart, A., Thalheimer, F.B., Huntscha, S., Sobotta, M.C., Moehrle, B., Brocks, D., Bayindir, I., Kaschutnig, P., et al. (2015). Exit from dormancy provokes DNA-damage-induced attrition in haematopoietic stem cells. Nature *520*, 549–552.

Yilmaz, O.H., Kiel, M.J., and Morrison, S.J. (2006). SLAM family markers are conserved among hematopoietic stem cells from old and reconstituted mice and markedly increase their purity. Blood *107*, 924–930.

Zha, S., Sekiguchi, J., Brush, J.W., Bassing, C.H., and Alt, F.W. (2008). Complementary functions of ATM and H2AX in development and suppression of genomic instability. Proc. Natl. Acad. Sci. USA *105*, 9302–9306.

Zhang, Q.S., Marquez-Loza, L., Eaton, L., Duncan, A.W., Goldman, D.C., Anur, P., Watanabe-Smith, K., Rathbun, R.K., Fleming, W.H., Bagby, G.C., et al. (2010). Fancd2-/- mice have hematopoietic defects that can be partially corrected by resveratrol. Blood *116*, 5140–5148.

Zhang, S., Yajima, H., Huynh, H., Zheng, J., Callen, E., Chen, H.T., Wong, N., Bunting, S., Lin, Y.F., Li, M., et al. (2011). Congenital bone marrow failure in DNA-PKcs mutant mice associated with deficiencies in DNA repair. J. Cell Biol. *193*, 295–305.

Zhang, Q.S., Watanabe-Smith, K., Schubert, K., Major, A., Sheehan, A.M., Marquez-Loza, L., Newell, A.E., Benedetti, E., Joseph, E., Olson, S., et al. (2013). Fancd2 and p21 function independently in maintaining the size of hematopoietic stem and progenitor cell pool in mice. Stem Cell Res. *11*, 687–692.

Zhang, H., Kozono, D.E., O'Connor, K.W., Vidal-Cardenas, S., Rousseau, A., Hamilton, A., Moreau, L., Gaudiano, E.F., Greenberger, J., Bagby, G., et al. (2016). TGF-beta inhibition rescues hematopoietic stem cell defects and bone marrow failure in Fanconi anemia. Cell Stem Cell *18*, 668–681.